Magnetic and neutron diffraction study on quaternary oxides MTeMoO$_6$ (M = Mn and Zn)

Magnetic and neutron diffraction study on quaternary oxides MTeMoO$_6$ (M = Mn and Zn)

Yoshihiro Doi[1,3], Ryo Suzuki[1], Yukio Hinatsu[1] and Kenji Ohoyama[2]

[1] Division of Chemistry, Graduate School of Science, Hokkaido University,
Sapporo 060-0810, Japan
[2] Institute for Materials Research, Tohoku University, Sendai 980-8577, Japan

E-mail: doi@sci.hokudai.ac.jp

Abstract
Crystal structures and magnetic properties of quaternary oxides MTeMoO$_6$ (M = Mn and Zn)
were investigated. From the Rietveld analyses for the powder x-ray and neutron diffraction
measurements, their detailed structures have been determined. Both compounds have
orthorhombic structure with space group $P2_12_12$ and a charge configuration of
$M^{2+}Te^{4+}Mo^{6+}O_6$. ZnTeMoO$_6$ shows diamagnetic behavior. In this structure, M ions are
arranged in a square-planar manner. The temperature dependence of the magnetic susceptibility
for MnTeMoO$_6$ shows a broad peak at $\sim$33 K, which is due to a two-dimensional characteristic
of the magnetic interaction. In addition, this compound shows an antiferromagnetic transition at
20 K. The magnetic structure was determined by the powder neutron diffraction measurement at
3.3 K. The magnetic moments of Mn^{2+} ions (4.45 μ_B) order in a collinear antiferromagnetic
arrangement along the b axis.

S Supplementary data are available from stacks.iop.org/JPhysCM/21/046006

1. Introduction

Quaternary oxides MTeMoO$_6$ (M = Mg, Mn, Co, Zn, Cd), the
so-called additive telluromolybdates, were first synthesized in
the latter half of the 1970s [1–8] and their catalytic properties
were investigated [1, 9–11]. The x-ray diffraction data for
these compounds were indexed in an orthorhombic unit cell
with space group $P2_12_12$ [1, 12], except for CdTeMoO$_6$ which
adopts a tetragonal unit cell [8]. However, their accurate
structural data was unknown for a long time. After about
two decades, Hayashi *et al* proposed the atomic positions of
three metal ions in CoTeMoO$_6$ [13], and Laligant determined
detailed structural parameters for the orthorhombic CoTeMoO$_6$
and tetragonal CdTeMoO$_6$ [14].

The schematic crystal structure of the orthorhombic
MTeMoO$_6$ is illustrated in figure 1(a). In this structure,
all the M ions are located at $z \sim 0.5$ and form a square-
planar lattice in the ab-plane (see figure 1(b)); the layers
consisting of MO$_6$ octahedra are separated by other layers
which are formed by MoO$_4$ tetrahedra and TeO$_4$ polyhedra.

If the M ion is magnetic, this compound can be seen as a
two-dimensional magnetic system. The materials in such a
system have been of great interest because of their unique
physical properties [15]. However, their magnetic properties
are not well known except for the effective magnetic moment
and Weiss constant for CoTeMoO$_6$ determined by magnetic
susceptibility measurements (T = 100–300 K) [16], and
no evidence for the long-range magnetic ordering has been
observed.

In this paper, we will report the detailed crystal structures
for MnTeMoO$_6$ and ZnTeMoO$_6$ determined by powder x-
ray and neutron diffraction measurements, and reveal the
magnetic properties of MnTeMoO$_6$ by magnetic susceptibility,
specific heat, and neutron diffraction measurements at low
temperatures.

2. Experimental details

2.1. Sample preparation

Two polycrystalline samples (MnTeMoO$_6$ and ZnTeMoO$_6$)
were prepared by the solid-state reaction. The ZnTeMoO$_6$ was

---

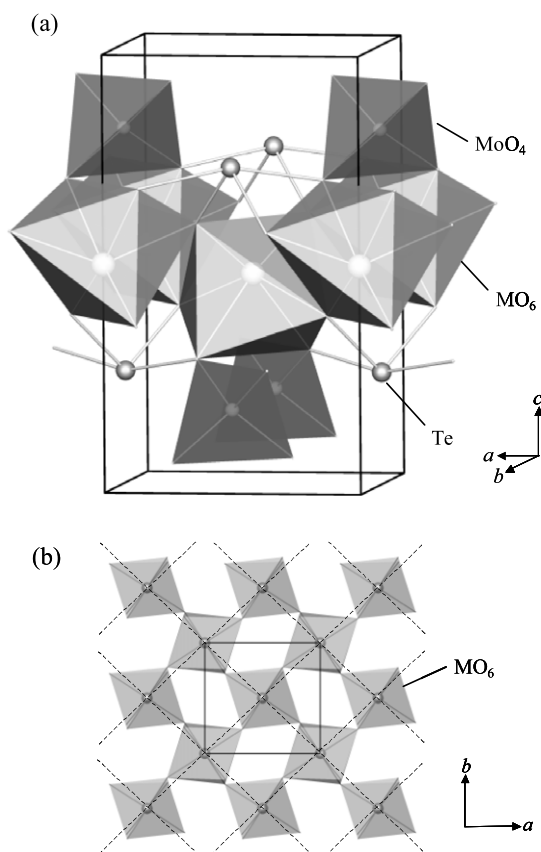[3] Author to whom any correspondence should be addressed.

Figure 1. (a) Schematic crystal structure of the orthorhombic MTeMoO$_6$ and (b) network of the MO$_6$ octahedra. In (b), the dashed lines represent the square-planar lattice of M ions.

Figure 2. Powder x-ray diffraction profiles for (a) MnTeMoO$_6$ and (b) ZnTeMoO$_6$. The calculated and observed diffraction profiles are shown on the top as a solid line and cross markers, respectively. The vertical markers show positions calculated from Bragg reflections. The bottom trace is a plot of the difference between the calculated and observed intensities.

needed to estimate the lattice and electronic contribution to the total specific heat for MnTeMoO$_6$, which will be described later. The starting materials, MnO, ZnO, TeO$_2$ and MoO$_3$ were weighed in appropriate metal ratios and ground intimately in an agate mortar. The mixtures were pressed into pellets, and then the pellet was sealed in an evacuated silica tube to prevent the loss of reagents by the volatilization. These ampules were heated at 873 K (for MnTeMoO$_6$) or 823 K (for ZnTeMoO$_6$) for 12×3 h with intermediate grinding and pelletizing.

2.2. Powder x-ray and neutron diffraction measurements

The powder x-ray diffraction (XRD) measurements were performed at room temperature in the range $10° \leqslant 2\theta \leqslant 120°$ using a 2θ step size of $0.02°$ with Cu Kα radiation on a Rigaku MultiFlex diffractometer. Powder neutron diffraction (ND) profiles were also measured for MnTeMoO$_6$ (at 3.3 K, 11 K and room temperature) and ZnTeMoO$_6$ (at room temperature) in the range $3° \leqslant 2\theta \leqslant 153°$ at intervals of $0.02°$ with a wavelength of $1.814\,24$ Å. Measurements were performed by the Kinken powder diffractometer for high efficiency and high resolution measurements, HERMES, of the Institute for Materials Research (IMR), Tohoku University [17], installed at the JRR-3M reactor in Japan Atomic Energy Agency (JAEA), Tokai. The x-ray and neutron diffraction data were analyzed by the Rietveld technique, using the program RIETAN2000 [18].
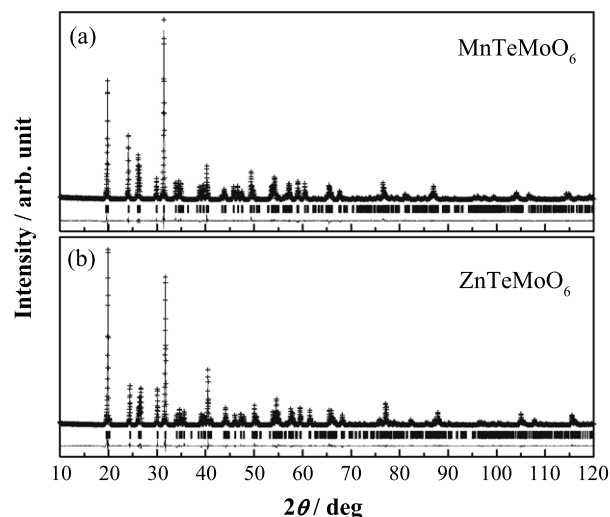
2.3. Magnetic susceptibility and specific heat measurements

The temperature dependence of the magnetic susceptibilities was measured under both zero-field-cooled (ZFC) and field-cooled (FC) conditions in an applied field of 0.1 T over the temperature range 1.8–400 K using a SQUID magnetometer (Quantum Design, MPMS-5S). In addition, specific heat measurements were performed using a relaxation technique with a commercial physical property measurement system (Quantum Design, PPMS model) in the temperature range 1.8–300 K. The sintered sample in the form of a pellet was mounted on a thin alumina plate with grease for better thermal contact.

3. Results and discussion

3.1. Crystal structure

The title compounds MnTeMoO$_6$ and ZnTeMoO$_6$ were successfully prepared as a single phase. Figure 2 shows their powder x-ray diffraction profiles. Both data were indexed with an orthorhombic unit cell ($a \sim 5.3$ Å, $b \sim 5.0$ Å, and $c \sim 8.9$ Å) with the space group $P2_12_12$ (No. 18), and analyzed by the Rietveld method using the structural model for CoTeMoO$_6$ [14]. The calculated profiles are plotted in figure 2, which gives a good agreement with the observed profiles. The obtained lattice parameters are consistent with those in earlier works [1, 12]. The structural parameters determined by XRD measurements are shown in supplementary tables (available at stacks.iop.org/JPhysCM/21/046006).

The powder neutron diffraction measurements were performed for MnTeMoO$_6$ (at 3.3 K, 11 K, and room temperature) and ZnTeMoO$_6$ (at room temperature). Their diffraction profiles are shown in figures 3 and 4, respectively. The Rietveld analyses of the data indicate that both compounds adopt the same structure as CoTeMoO$_6$ [14], and are consistent
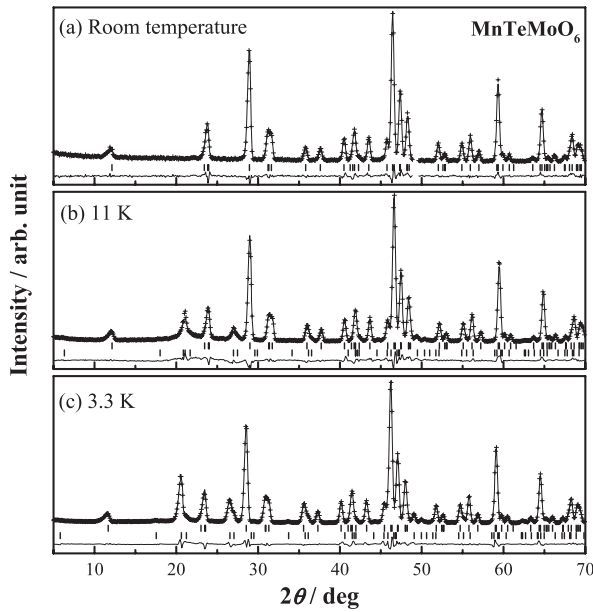
Figure 3. Powder neutron diffraction profiles for $MnTeMoO_6$ (a) at room temperature, (b) at 11 K, and (c) at 3.3 K. The calculated and observed diffraction profiles are shown on the top as a solid line and cross markers, respectively. The upper vertical markers show positions calculated from nuclear Bragg reflections, and in (b) and (c) the lower ones show those from magnetic Bragg reflections. The bottom trace is a plot of the difference between the calculated and observed intensities.
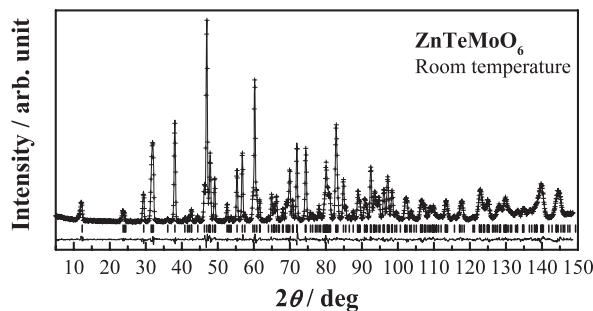

Figure 4. Powder neutron diffraction profile for $ZnTeMoO_6$ at room temperature. The calculated and observed diffraction profiles are shown on the top as a solid line and cross markers, respectively. The vertical markers show positions calculated from nuclear Bragg reflections. The bottom trace is a plot of the difference between the calculated and observed intensities.

Table 1. Structural parameters for $MnTeMoO_6$ determined by powder neutron diffraction measurements.

Atom	Site	x	y	z	B (Å^2)
Room temperature, space group $P2_12_12$; $a = 5.2941(3)$ Å, $b = 5.1350(3)$ Å, $c = 8.9544(5)$ Å, $R_{wp} = 6.45\%$, $R_p = 5.06\%$, $R_e = 4.75\%$, $R_I = 1.01\%$.
Mn	2a	0	0	0.5229(7)	0.89(9)
Te	2b	0	1/2	0.2497(5)	0.59(9)
Mo	2b	0	1/2	0.8102(4)	0.52(8)
O1	4c	0.2986(5)	0.8391(5)	0.0722(3)	1.02(7)
O2	4c	0.1895(5)	0.7478(6)	0.7086(3)	0.77(7)
O3	4c	0.1773(6)	0.7108(5)	0.3867(3)	0.90(7)
$T = 11$ K, space group $P2_12_12$; $a = 5.2850(3)$ Å, $b = 5.1198(2)$ Å, $c = 8.9132(4)$ Å, $R_{wp} = 7.40\%$, $R_p = 5.40\%$, $R_e = 2.77\%$, $R_I(\text{crystal}) = 1.56\%$, $R_I(\text{magnetic}) = 1.53\%$, $\mu_{Mn} = 2.71(2)\mu_B$.
Mn	2a	0	0	0.5227(6)	0.14(9)
Te	2b	0	1/2	0.2486(4)	0.29(8)
Mo	2b	0	1/2	0.8111(4)	0.22(7)
O1	4c	0.2972(5)	0.8394(5)	0.0712(3)	0.44(5)
O2	4c	0.1877(5)	0.7500(5)	0.7093(3)	0.26(5)
O3	4c	0.1781(5)	0.7133(4)	0.3862(3)	0.43(5)
$T = 3.3$ K, space group $P2_12_12$; $a = 5.2846(2)$ Å, $b = 5.1195(2)$ Å, $c = 8.9119(4)$ Å, $R_{wp} = 5.34\%$, $R_p = 3.82\%$, $R_e = 1.82\%$, $R_I(\text{crystal}) = 0.95\%$, $R_I(\text{magnetic}) = 1.98\%$, $\mu_{Mn} = 4.46(2)\mu_B$.
Mn	2a	0	0	0.5227(3)	0.09(9)
Te	2b	0	1/2	0.2483(3)	0.21(6)
Mo	2b	0	1/2	0.8120(3)	0.20(6)
O1	4c	0.2970(4)	0.8400(4)	0.0710(2)	0.45(5)
O2	4c	0.1879(4)	0.7492(4)	0.7086(2)	0.37(5)
O3	4c	0.1775(4)	0.7128(3)	0.3863(2)	0.40(5)

Table 2. Structural parameters for $ZnTeMoO_6$ determined by powder neutron diffraction measurements at room temperature. (Note: space group $P2_12_12$; $a = 5.2630(2)$ Å, $b = 5.0426(3)$ Å, $c = 8.9105(4)$ Å, $R_{wp} = 5.60\%$, $R_p = 4.29\%$, $R_e = 4.04\%$, $R_I = 0.90\%$.)

Atom	Site	x	y	z	B (Å^2)
Zn	2a	0	0	0.5218(4)	0.46(7)
Te	2b	0	1/2	0.2553(3)	0.56(7)
Mo	2b	0	1/2	0.8088(3)	0.46(7)
O1	4c	0.2891(4)	0.8467(4)	0.0745(3)	1.13(6)
O2	4c	0.1805(5)	0.7612(4)	0.7067(2)	0.77(6)
O3	4c	0.1746(4)	0.7213(4)	0.3933(2)	0.66(6)

with the results of the XRD data. Evidence of the occurrence of cation disorder or an oxygen defect has not been found; all the occupancy parameters were fixed to 1.0. For $MnTeMoO_6$, the data collected at 3.3 and 11 K show a number of low-angle peaks, which are not observed at room temperature. As will be discussed later, they are due to an antiferromagnetic ordering of Mn^{2+} moments. The crystal structures at 3.3 and 11 K have the same symmetry as that at room temperature; thus, no structural transition occurs. The refined structural parameters for $MnTeMoO_6$ and $ZnTeMoO_6$ are summarized in tables 1 and 2, respectively.

The crystal structure of the orthorhombic $MTeMoO_6$ is illustrated in figure 1(a). In this structure, M ions form a square-planar lattice with 3.71 Å on a side for M = Mn and 3.66 Å for Zn (see figure 1(b)). This lattice is very close to a regular one but somewhat uneven (± 0.2 Å from the horizontal level) because M ions locate in the 2a site: $(0, 0, z)$ and $(1/2, 1/2, 1-z)$ with $z \sim 0.52$. The distance between adjacent layers of M ions ($c = 8.91$–8.95 Å) is much longer than the distance of the nearest M–M. Therefore, $MnTeMoO_6$ is appropriate to observe a two-dimensional magnetic behavior.

The coordination around the M ion is shown in figure 5(a), and interatomic distances are listed in table 3. The M ion is surrounded by eight oxygen ions; among them, six oxygen ions with shorter M–O lengths (2.0–2.3 Å) form a distorted MO_6 octahedron, and the other two have longer M–O lengths
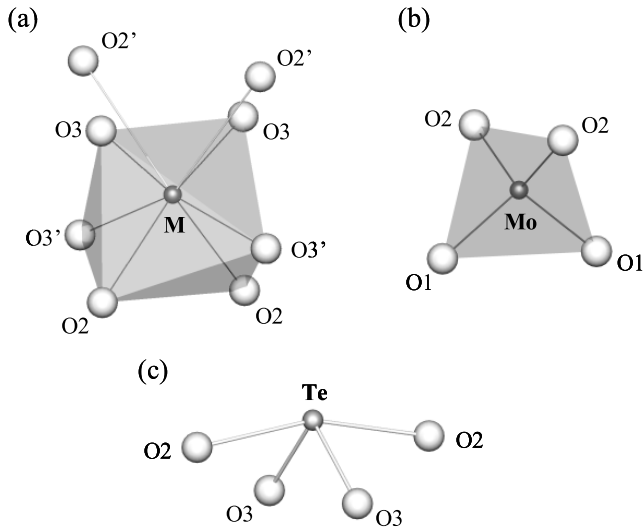
3

Figure 5. Coordination environments around (a) M, (b) Mo, and (c) Te ions in the orthorhombic MTeMoO$_6$.

Table 3. Selected interatomic distances (Å) and bond valence sums determined by neutron diffraction measurements.

	ZnTeMoO$_6$ RT	MnTeMoO$_6$ RT	MnTeMoO$_6$ 3.3 K
M–O3 × 2	2.033(3)	2.139(5)	2.126(3)
M–O3′ × 2	2.180(2)	2.179(4)	2.179(2)
M–O2 × 2	2.251(3)	2.334(5)	2.319(3)
M–O2′ × 2	2.951(3)	2.935(5)	2.932(3)
BVS	1.90	2.03	2.08
Te–O3 × 2	1.897(3)	1.886(3)	1.892(3)
Te–O2 × 2	2.096(3)	2.126(3)	2.125(2)
Te–O1 × 2	2.823(3)	2.839(3)	2.827(2)
Te–O1′ × 2	3.297(4)	3.184(5)	3.150(3)
BVS	4.19	4.17	4.14
Mo–O1 × 2	1.706(3)	1.711(4)	1.705(3)
Mo–O2 × 2	1.861(3)	1.859(3)	1.861(2)
Mo–O3 × 2	2.855(3)	2.869(4)	2.862(3)
Mo–O1′ × 2	3.313(3)	3.322(3)	3.290(2)
BVS	5.90	5.87	5.92

(~2.9 Å). The bond valence sums (BVSs) calculated from the determined interatomic distances are 2.03 for M = Mn and 1.90 for Zn, which are reasonable values for divalent M ions.

　　The coordination environments around Mo and Te ions are illustrated in figures 5(b) and (c), respectively. The metal–oxygen distance and BVS are also listed in table 3. The values of BVS are reasonable to the hexavalent Mo and tetravalent Te ions. The interatomic distances indicate that both ions occupy four-coordinated sites; however, the way of the coordination is considerably different between them. The Mo^{6+} ion is surrounded by four oxygen ions with a normal tetrahedral arrangement, while the Te^{4+} ion protrudes from a polyhedron consisting of four oxygen ions, and the upper side of the Te ion is unoccupied as shown in figure 5(c). The latter is due to the existence of lone pair electrons. Similar coordination environments are often observed for Te^{4+} compounds, e.g. CoTeMoO$_6$ [14], Co$_6$Te$_5$O$_{16}$ [19], and Ln$_2$Te$_4$O$_{11}$ (Ln = lanthanides) [20].
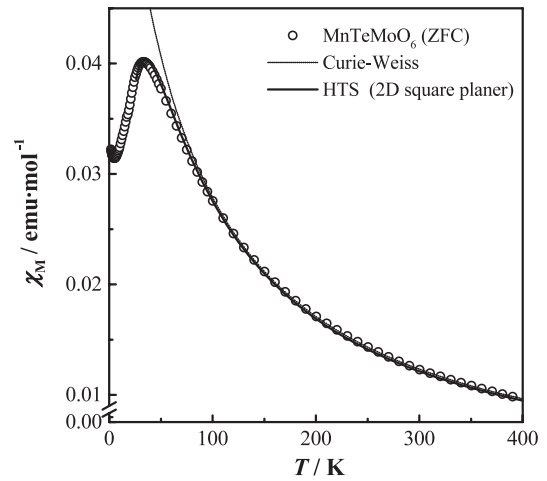

Figure 6. Temperature dependence of the ZFC magnetic susceptibility for MnTeMoO$_6$. The dotted and solid curves represent the calculated susceptibilities by using the Curie–Weiss law and high temperature series (HTS) expansion for a square-planar lattice, respectively.

3.2. Magnetic susceptibility

The magnetic susceptibility of ZnTeMoO$_6$ is diamagnetic and temperature-independent ($\sim$−1.3 × 10^{-4} emu mol^{-1}) in the experimental temperature range (1.8–400 K). This behavior corresponds to experimental results in the structural analysis: the valence configuration Zn^{2+}Te^{4+}Mo^{6+}O$_6$ and no oxygen defect.

　　Figure 6 shows the temperature dependence of the ZFC magnetic susceptibility for MnTeMoO$_6$. The data in the higher temperature region (T > 100 K) were fitted by the Curie–Weiss law; the effective magnetic moment (μ_{eff}) and Weiss constant (θ) were determined to be 5.95(1) μ_{B} and −58.8(6) K, respectively. This magnetic moment is in good agreement with the free-ion value (5.92 μ_{B}) of the Mn^{2+} ion in the high-spin state ($S = 5/2$). The negative Weiss constant suggests that the predominant magnetic interaction between Mn ions is antiferromagnetic.

　　At lower temperatures, the deviation from the Curie–Weiss curve becomes larger and the magnetic susceptibility shows a broad maximum at around 33 K. This behavior may be due to the two-dimensional nature of the magnetic interaction. In this compound, the arrangement of the magnetic Mn^{2+} ions is regarded as the square-planar lattice; thus, we have fitted the observed magnetic susceptibility using a high temperature series (HTS) expansion of the square-planar lattice for the Heisenberg model:

$$\chi_{\text{M}} = \frac{N_A g^2 \mu_{\text{B}}^2 S(S+1)}{3 k_{\text{B}} T} \sum a_n (J/k_{\text{B}} T)^n \qquad (1)$$

where N_{A}, g, μ_{B}, k_{B}, and J are the Avogadro number, g factor, Bohr magneton, Boltzmann constant, and exchange integral, respectively. We used the coefficients a_n (n = 1–8) given in previous results [15, 21–24]. The fitting equation was obtained by applying the Padé approximation ([4,4] Padé) to the equation (1). The calculated susceptibility is shown
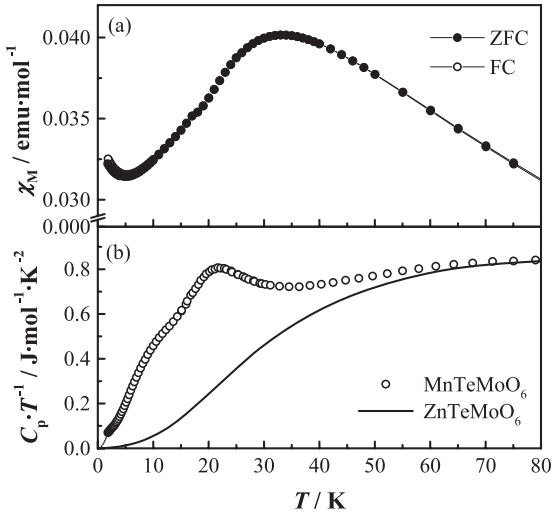
Figure 7. Temperature dependence of (a) the ZFC and FC magnetic susceptibilities for MnTeMoO$_6$ and (b) specific heat divided by temperature for MnTeMoO$_6$ and ZnTeMoO$_6$.

Figure 8. Temperature dependence of (a) the magnetic specific heat divided by temperature and (b) magnetic entropy for MnTeMoO$_6$.

as a solid line in figure 6, and it is in good agreement with the experimental data. The g factor of the Mn^{2+} ion and exchange integral J for the nearest Mn–Mn in the square-planar lattice are determined to be 1.95(1) and $-1.96(1)$ K, respectively. The Weiss constant calculated from only this J value ($\sum_i 2z_i J_i S(S+1)/3k_B$; $z=4$) is -45.7 K, which is comparable to the value estimated from the Curie–Weiss law (-58.8 K).

The ZFC and FC magnetic susceptibilities for MnTeMoO$_6$ at low temperatures are plotted in figure 7(a). In addition to the broad peak at 33 K, they show a small anomaly at ~17 K, and a slight divergence between ZFC and FC data is observed below this temperature, indicating the existence of a small ferromagnetic moment ~10^{-4} μ_B. In order to obtain further information about the magnetic properties of this compound, specific heat measurements were carried out.

3.3. Specific heat

The temperature dependence of the specific heat divided by temperature (C_p/T) for MnTeMoO$_6$ is plotted in figure 7(b). The data show a broad λ-type anomaly at 20 K, which indicates that long-range antiferromagnetic ordering of Mn^{2+} ions occurs. This result corresponds to the divergence between ZFC and FC magnetic susceptibilities. A small ferromagnetic moment observed in the magnetization measurement may be due to a weak ferromagnetic component associated with the antiferromagnetism caused by the Dzyaloshinsky–Moriya (DM) interaction, which is often observed in compounds with lower crystal symmetry.

The magnetic entropy change (ΔS_{mag}) associated with the antiferromagnetic transition was calculated by using $\Delta S_{mag} = \int (C_{mag}/T)dT$, in which the magnetic specific heat (C_{mag}) was estimated by subtracting the lattice and electronic specific heat from the experimental specific heat of MnTeMoO$_6$. For the lattice and electronic contributions, we used the specific heat of a nonmagnetic and isostructural compound ZnTeMoO$_6$
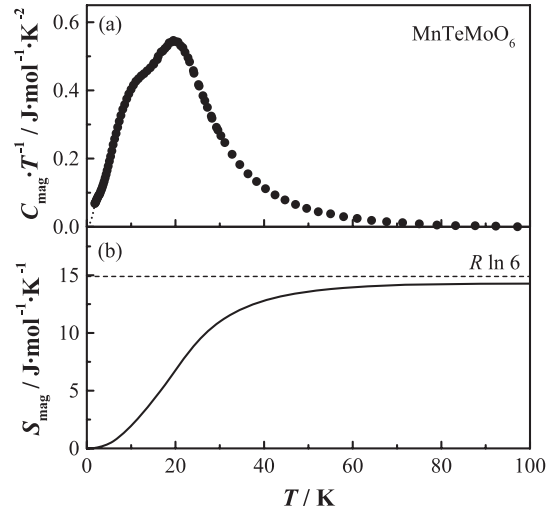
(the data are shown as a solid line in figure 7(b)). The temperature dependences of the magnetic specific heat divided by temperature (C_{mag}/T) and magnetic entropy (S_{mag}) are plotted in figures 8(a) and (b), respectively. Above 20 K, the peak of C_{mag}/T data shows a long tail up to ~70 K. This result indicates that the short-range magnetic ordering in the 2D layer of Mn^{2+} ions begins at a much higher temperature than the transition temperature. The ΔS_{mag} associated with the antiferromagnetic transition reaches 14.3 J mol^{-1} K^{-1} at 100 K, which is in good agreement with the value expected from the sixfold-degenerated ground state of the high-spin 3d^5 ion ($R\ln 6 = 14.90$ J mol^{-1} K^{-1}).

3.4. Magnetic structure

Powder neutron diffraction measurements for MnTeMoO$_6$ were carried out below the magnetic transition temperature. The ND profiles collected at 11 and 3.3 K are plotted in figures 3(b) and (c), respectively. Both data show a number of low-angle peaks, which were associated with the antiferromagnetic transition found in the magnetic susceptibility and specific heat measurements. All these reflections can be indexed using a propagation vector $k = (0, 0, 1/2)$, i.e. the magnetic unit cell is represented as $a_{mag} = a$, $b_{mag} = b$, and $c_{mag} = 2c$. To determine the magnetic structure, we have tested many models expected from the symmetry of the crystal structure and the propagation vector, and finally found that a collinear antiferromagnetic structure gave a good calculation result. The calculated profiles are plotted as the solid line in figures 3(b) and (c). The ferromagnetic component expected from the result of the magnetic susceptibility measurement is too small to be detected.

The magnetic structure determined for MnTeMoO$_6$ is illustrated in figure 9. All the magnetic moments of Mn ions are collinear along the b axis. In the ab plane, the nearest Mn moments order antiferromagnetically via the superexchange Mn–O3–Mn or longer Mn–O2–Mn pathways. The ordered
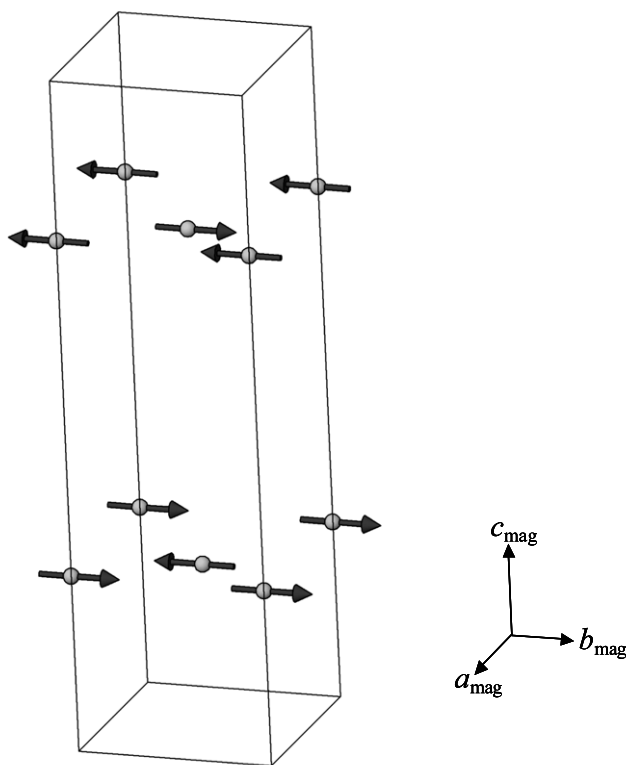
Figure 9. Magnetic structure of MnTeMoO$_6$. Diamagnetic ions are omitted. Arrows represent the direction of magnetic moments for Mn^{2+} ions.

magnetic moment for the Mn^{2+} ion is determined to be 4.45(1) μ_B at 3.3 K, which is in good agreement with the 5 μ_B expected from the 3d^5 electronic configuration in the high-spin state ($S = 5/2$).

4. Summary

Quaternary compounds MnTeMoO$_6$ and ZnTeMoO$_6$ adopt the orthorhombic structure with space group $P2_12_12$, and their detailed structural parameters have been determined by Rietveld analyses for powder x-ray and neutron diffraction measurements. The MnTeMoO$_6$ shows characteristic magnetic properties as a two-dimensional magnet reflecting the arrangement of Mn ions (square-planar lattice). In addition,

this compound shows a long-range antiferromagnetic ordering of Mn^{2+} moments at 20 K with a collinear antiferromagnetic arrangement along the *b* axis.

Acknowledgments

References

[1] Forzatti P and Tittarelli P 1980 *J. Solid State Chem.* **33** 421–7
[2] Botto I L and Baran E J 1980 *Z. Anorg. Allg. Chem.* **468** 221–7
[3] Forzatti P and Trifirò F 1977 *Gazz. Chim. Ital.* **107** 259–61
[4] Kozłowski R and Słoczyński J 1976 *J. Solid State Chem.* **18** 51–5
[5] Forzatti P 1978 *Gazz. Chim. Ital.* **108** 73–5
[6] Słoczyński J and Śliwa B 1978 *Z. Anorg. Allg. Chem.* **438** 295–304
[7] Forzatti P and Trifirò F 1977 *Gazz. Chim. Ital.* **107** 35–7
[8] Forzatti P and Tieghi G 1978 *J. Solid State Chem.* **25** 387–90
[9] Forzatti P, Trifirò F and Villa P L 1978 *J. Catal.* **55** 52–7
[10] Forzatti P and Trifirò F 1979 *React. Kinet. Catal. Lett.* **10** 275–80
[11] Hayashi H, Sugiyama S, Kokawa N and Koto K 1997 *Appl. Surf. Sci.* **121/122** 378–81
[12] Tieghi G and Forzatti P 1978 *J. Appl. Crystallogr.* **11** 291–2
[13] Hayashi H, Kokawa N, Moriga T, Sugiyama S and Koto K 1999 *J. Mol. Catal.* A **145** 301–7
[14] Laligant Y 2001 *J. Solid State Chem.* **160** 401–8
[15] de Jongh L J (ed) 1989 *Magnetic Properties of Layered Transition Metal Compounds* (Dordrecht: Kluwer–Academic)
[16] Botto I L, Baran E J and Minelli G 1984 *Solid State Commun.* **50** 693–5
[17] Ohoyama K, Kanouchi T, Nemoto K, Ohashi M, Kajitani T and Yamaguchi Y 1998 *Japan. J. Appl. Phys.* **37** 3319–26
[18] Izumi F and Ikeda T 2000 *Mater. Sci. Forum* **321–324** 198–203
[19] Trömel M and Scheller Th 1976 *Z. Anorg. Allg. Chem.* **427** 229–34
[20] Mayer H and Weil M 2003 *Z. Anorg. Allg. Chem.* **629** 1068–72
[21] Rushbrooke G S and Wood P J 1955 *Proc. Phys. Soc. Lond.* **68** 1161–9
[22] Rushbrooke G S and Wood P J 1958 *Mol. Phys.* **1** 257–83
[23] Stephenson R L, Pirnie K, Wood P J and Eve J 1968 *Phys. Lett.* A **27** 2–3
[24] Yamaji K and Kondo J 1973 *J. Phys. Soc. Japan* **35** 25–32